Research Square

Preprints are preliminary reports that have not undergone peer review.
They should not be considered conclusive, used to inform clinical practice,
or referenced by the media as validated information.

Spatial variation in long-term natural recovery potential informs targeted post-fire restoration in a peri-urban forest

Yuanting Yang
Chongqing University
Hongyan Xiao
Yangtze Normal University
Jie Lei
Chongqing University
Chunlan Du
Chongqing University
Bo Li
elaplibo@cqu.edu.cn
Chongqing University

Research Article

Keywords: peri-urban forest, post-fire restoration, succession modeling, LANDIS-II, wildfire

Posted Date: November 11th, 2026

DOI: https://doi.org/10.21203/rs.3.rs-11243692/v1

License: This work is licensed under a Creative Commons Attribution 4.0 International License.
Read Full License

Additional Declarations: No competing interests reported.

Spatial variation in long-term natural recovery potential informs targeted post-fire restoration in a peri-urban forest

Yuanting Yang [1], Hongyan Xiao [2], Jie Lei [1], Chunlan Du [1,3], Bo Li [1,3,*]

[1] School of Architecture and Urban Planning, Chongqing University, Chongqing 400030, China

[2] Green Intelligence Environmental School, Yangtze Normal University, Chongqing 408100, China

[3] Key Laboratory of New Technology for Construction of Cities in Mountain Area, Chongqing University, Chongqing 400030, China

*** Corresponding author: Bo Li**

Email: elaplibo@cqu.edu.cn

ORCID: 0000-0001-9712-9561

Statements and Declarations

- Funding

This work was supported by the National Natural Science Foundation of China: the Key Program [grant number 52238003]; and the General Program [grant number 52078074].

- Competing Interests

The authors have no relevant financial or non-financial interests to disclose.

- Ethics approval

Not applicable.

- Consent to participate

Not applicable.

- Consent for publication

Not applicable.

- Data Availability

The datasets analyzed during the current study are available from the corresponding author on reasonable request.

- Code availability

The code used in the current study is available from the corresponding author on reasonable request.

- Authors' contributions

YY, BL conceived and designed the research; YY performed the analyses and prepared the figures; HX, JL, CD contributed field data and interpretation; YY drafted the manuscript; BL, HX, JL, CD reviewed and edited the manuscript.

Abstract

Post-fire recovery capacity can vary substantially within peri-urban forests, where heterogeneous environmental conditions complicate decisions about when natural regeneration is sufficient and where active intervention is warranted. We evaluated spatial variation in long-term natural recovery potential and the effects of targeted planting in a fire-affected peri-urban forest in Jinyun Mountain, Chongqing, China. Unmanned aerial vehicle (UAV) multispectral imagery, U-Net classification, and field observations were integrated to reconstruct post-fire vegetation conditions, which were used to initialize 100-year LANDIS-II simulations under natural succession (S1) and spatially targeted planting (S2). A Restoration Potential Index (RPI), derived exclusively from year-100 S1 outputs, integrated structural recovery, ecosystem productivity, and community development to identify spatial differences in modeled natural recovery potential. Recovery potential was strongly heterogeneous across the burned landscape, while bamboo showed sustained biomass expansion under natural succession. Targeted planting produced higher simulated aboveground carbon stocks and earlier biomass and aboveground net primary productivity (ANPP) breakpoints than natural succession, with estimated advances of approximately 9 and 10 years, respectively. However, scenario differences narrowed during later succession, and diversity responses were modest and spatially variable. These results indicate that post-fire restoration in heterogeneous peri-urban forests may benefit from spatially differentiated management: active planting can be concentrated in areas with relatively low natural recovery potential, whereas higher-recovery areas may rely

more strongly on passive succession and continued monitoring.

Keywords: peri-urban forest; post-fire restoration; succession modeling; LANDIS-II; wildfire

1 Introduction

Forest ecosystems provide essential ecosystem services, including carbon sequestration, biodiversity conservation, and climate regulation, and are particularly important for maintaining ecological functions in rapidly urbanizing regions (Bonan 2008). Increasing wildfire frequency, intensity, and extent under climate change and human pressures have substantially altered forest structure and ecosystem functioning (van Lierop et al. 2015; Huang et al. 2021; Heidari et al. 2021). Wildfire disturbance can directly reduce vegetation cover and biomass and subsequently affect forest regeneration, soil stability, air quality, and other ecosystem services (Viana-Soto et al. 2020; Alayan et al. 2022). These effects can be particularly consequential in peri-urban forests and wildland-urban interface (WUI) areas, where ecological recovery occurs close to human settlements and post-fire management must maintain ecosystem functions while allocating limited restoration resources (Ghermandi et al. 2016; Thompson et al. 2017; Escobedo et al. 2024). Effective post-fire management of peri-urban forests therefore requires not only an understanding of ecological succession but also spatially explicit information that can support differentiated restoration decisions.

Ecological restoration is commonly defined as the process of assisting the recovery of ecosystems that have been degraded, damaged, or destroyed (Gerwing et al. 2022). In post-fire landscapes, however, ecosystem recovery capacity is rarely spatially uniform. Even within a single fire event, different locations may follow contrasting successional trajectories because of variation in disturbance severity, vegetation composition, resource availability, topography, and post-fire management (Sithole et al. 2018; Blanco-Rodriguez et al. 2023). Consequently, post-fire restoration typically spans a continuum from passive restoration based primarily on natural succession to active restoration involving direct human intervention (Alayan et al. 2022). Recent restoration concepts, including Nature-based Solutions (Regos 2026; Alberti et al. 2026) and future-oriented restoration (FaBRestor) frameworks (Montemagni et al. 2026), have gradually become important references for restoration after disturbance, putting forward higher requirements for conforming to the natural succession process of forests. Passive restoration may be appropriate where surviving vegetation and site conditions provide sufficient capacity for recovery (White and Long 2019; Alayan et al. 2022), whereas active intervention may be more justified where disturbance is severe or natural regeneration is expected to be slow (Mantero et al. 2024; Rodman et al. 2024). The central restoration question is therefore not simply whether a burned forest should be restored, but where intervention is necessary, where natural recovery may be sufficient, and whether the benefits of intervention persist over time.

Addressing this question requires information that links current post-fire

conditions with longer-term successional potential. Field surveys provide detailed information on vegetation composition and structure but are labor-intensive and spatially limited (Mitri and Gitas 2010). Satellite and airborne remote sensing can efficiently characterize burned areas and vegetation recovery across broader extents, but their capacity to resolve fine-scale vegetation structure and species-level patterns can be limited in heterogeneous forest landscapes (Chen et al. 2022; Sankey et al. 2024). High-resolution unmanned aerial vehicle (UAV) imagery can help bridge this scale gap by capturing fine spatial variation in post-fire vegetation, while deep-learning approaches can assist in extracting ecologically meaningful vegetation information from complex imagery (Viana-Soto et al. 2020; Avetisyan et al. 2022). However, such observations primarily describe current conditions and cannot alone determine whether a site is likely to recover naturally over decades. Forest landscape models, including LANDIS-II and LANDIS PRO, provide a complementary approach by simulating vegetation establishment, growth, dispersal, competition, and replacement over large spatial and temporal scales. Their usefulness for restoration planning depends, however, on realistic representation of initial vegetation conditions, species composition, site characteristics, and model parameterization (Xiao et al. 2017; Zhou et al. 2018).

A further challenge is translating long-term ecological trajectories into restoration priorities that can be used in practice. Model outputs such as biomass, productivity, and species composition can reveal ecological change but do not directly indicate where passive restoration may be sufficient or where active intervention

should be prioritized. Spatially explicit restoration planning therefore requires approaches that synthesize multiple dimensions of recovery into interpretable information capable of supporting decisions about intervention intensity and location (Busbridge et al. 2021; Rudge et al. 2022). This challenge is particularly relevant in heterogeneous peri-urban forests, where management resources must be allocated across landscapes that simultaneously contribute to urban ecological functions and experience spatially variable disturbance and regeneration conditions. Combining fine-scale ecological observations with succession modeling may therefore help move post-fire assessment beyond descriptions of current condition toward evaluation of relative long-term natural recovery potential and the expected benefits of intervention.

In this study, we examined a fire-affected peri-urban forest landscape in Jinyun Mountain, Chongqing, China. UAV multispectral imagery and U-Net semantic segmentation were used to characterize post-fire vegetation, while field observations and local floristic information were integrated to construct a field-informed species-level spatial initialization for the LANDIS-II landscape succession model. We then simulated 100-year post-fire succession under a natural-succession scenario and a spatially targeted planting scenario. Based exclusively on the natural-succession simulation, we developed a Restoration Potential Index (RPI) integrating structural recovery, ecosystem productivity, and community development to characterize spatial variation in long-term natural recovery potential. We addressed three questions: (1) How does long-term natural recovery potential vary spatially across a heterogeneous peri-urban mountain forest? (2) How can this spatial variation inform the allocation of

passive and active post-fire restoration? and (3) Does spatially targeted planting accelerate ecosystem recovery relative to natural succession, and are these benefits sustained over long successional periods? By addressing these questions, we aim to provide a spatially explicit basis for differentiated post-fire restoration and management in heterogeneous peri-urban forest ecosystems.

2 Methods

2.1 Study area and workflow

Jinyun Mountain National Nature Reserve is located on the northern edge of the central urban area of Chongqing, southwestern China, and forms an important peri-urban ecological buffer for this mountainous city. The region has a humid subtropical monsoon climate, with a mean annual temperature of 13.6 ° C and mean annual precipitation of 1,611.8 mm (Wang et al. 2023). Vegetation is dominated by subtropical evergreen broad-leaved forest, and the reserve supports high plant diversity and provides multiple ecosystem services to the surrounding urban area, including water conservation, climate regulation, air-quality regulation, and recreation.

A major wildfire began in Hutou Village, Jinyun Mountain, on 21 August 2022 and lasted for approximately five days. Approximately 1,400 ha were affected. The present study focused on the burned landscape within Jinyun Mountain, and the study boundary was delineated through preliminary interpretation of Sentinel-2 imagery (Fig. 1).

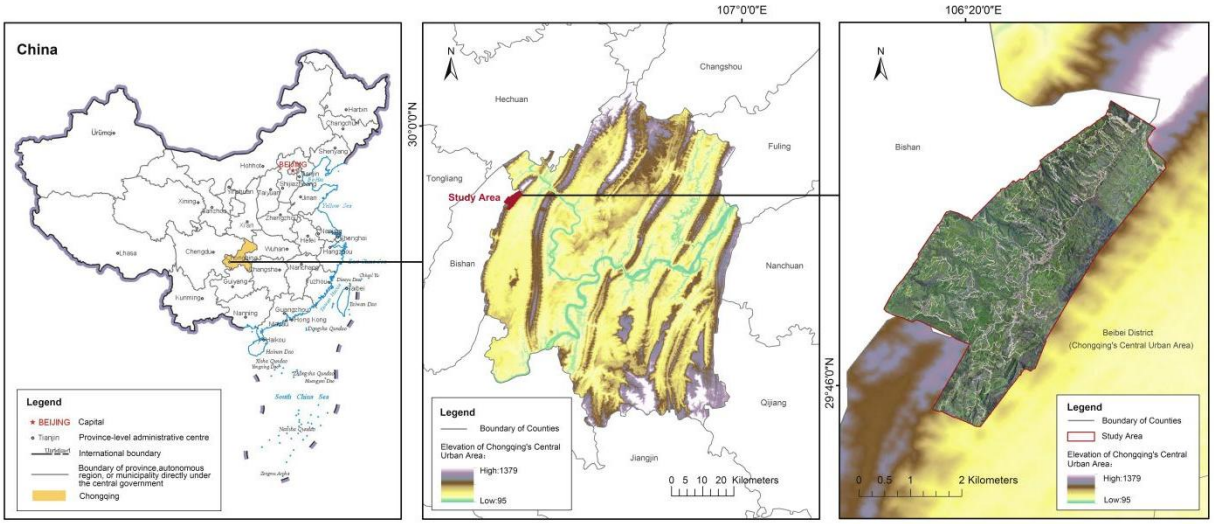


Fig. 1 Location of the Jinyun Mountain study area and its spatial relationship to Chongqing's central urban area

174

175 The workflow comprises three components: (1) UAV- and field-based
176 characterization of post-fire vegetation and topographic conditions; (2) LANDIS-II
177 simulation of long-term forest succession and assessment of spatial natural recovery
178 potential; and (3) comparison of natural succession and spatially targeted planting
179 (Fig. 2).

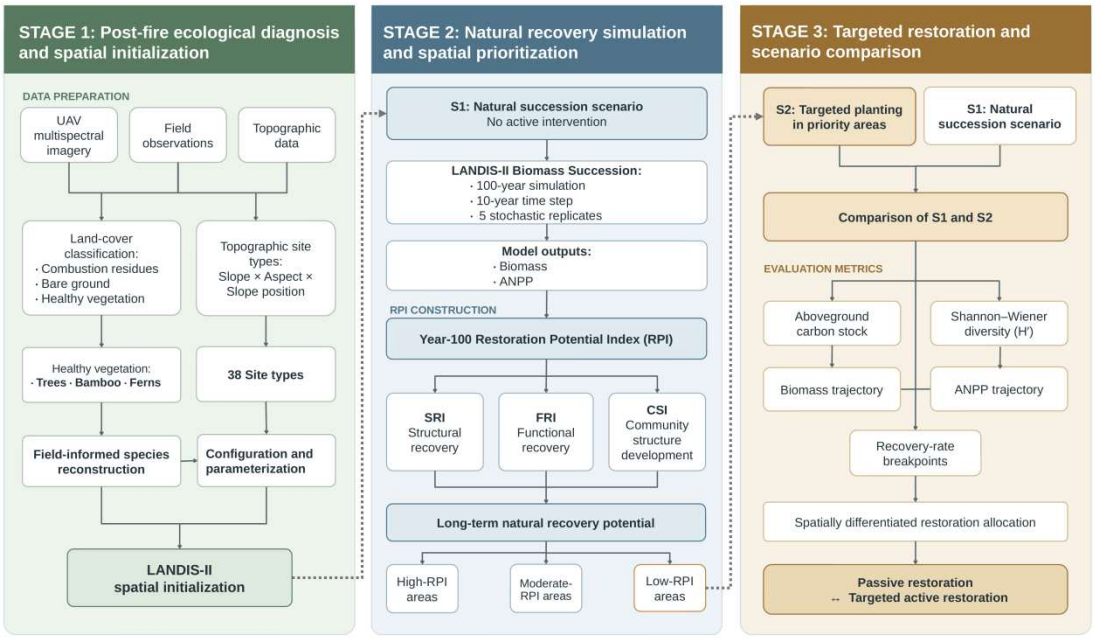


Fig. 2 Integrated study workflow

2.2 Post-fire vegetation and topographic data

Multispectral UAV imagery was acquired across the study area in May 2024 using a DJI Mavic 3M equipped with a multispectral imaging system. The imagery was processed in DJI Terra to generate a digital orthophoto mosaic (DOM), digital surface model (DSM), normalized difference vegetation index (NDVI), and three-dimensional oblique photogrammetric products. These datasets were subsequently used to characterize post-fire vegetation conditions and derive topographic variables for landscape-model initialization.

2.2.1 Land cover and vegetation classification

NDVI was first used to delineate the major land-cover conditions within the burned area. Following site-specific thresholds previously established using the same Jinyun Mountain post-fire UAV dataset (Li et al. 2026), three broad land-cover

categories were identified: combustion residues (0.25 < NDVI < 0.74), healthy vegetation (NDVI > 0.74), and bare ground (NDVI < 0.25) (Cui et al. 2024). This classification was used to separate vegetated areas from severely burned or non-vegetated surfaces.

Within vegetated areas, a U-Net semantic segmentation model was used to delineate the spatial distribution of three major vegetation groups: trees, bamboo, and ferns (Li et al. 2026). The model achieved an overall accuracy (OA) of 84.02%, mean precision of 84.21%, mean recall of 82.30%, macro-averaged F1 score (Macro-F1) of 83.11%, and mean intersection over union (mIoU) of 71.43%. The resulting vegetation map was subsequently used as spatial context for model initialization.

2.2.2 Topographic factors extraction and classification

Slope, aspect, and slope position were derived from the UAV-based DEM and DSM in ArcMap. Slope was classified into four categories according to the Forestry Industry Standards of the People's Republic of China and local site conditions: gentle ($0 \leqslant$ slope $< 14°$), steep ($14 \leqslant$ slope $< 34°$), abrupt ($34 \leqslant$ slope $< 44°$), and hazardous (slope $\geqslant 44°$). Aspect was classified as shady, semi-shady, or sunny, and slope position was classified as valley, ridge, lower slope, middle slope, or upper slope. These variables were subsequently combined to characterize spatial variation in site conditions relevant to species establishment and growth.

2.3 LANDIS-II spatial initialization and scenario design

The LANDIS-II landscape modeling framework (Scheller et al. 2007) was used

to simulate the long-term dynamics of post-fire forest succession under contrasting restoration scenarios.

2.3.1 Species composition and spatial initialization

The U-Net classification described above was used to identify the spatial distribution of major post-fire vegetation groups, including surviving trees, bamboo, and ferns. In tree-dominated areas, field vegetation surveys were conducted in September 2024 to record the locations and dominant identities of surviving plant species. These observations provided the primary reference for species assignment. Six species were represented in the tree-dominated areas: *Pinus massoniana*, *Pterocarya stenoptera*, *Quercus fabri* Hance, *Castanopsis fargesii*, *Schima superba*, *Machilus nanmu*. Because field observations consisted of discrete sampling locations, species-specific patches were manually delineated in ArcGIS by integrating the field records with canopy characteristics, vegetation texture, and spatial continuity visible in the high-resolution UAV orthophotos. A vegetation distribution map from the surrounding Jinyun Mountain area, the *Flora of Jinyun Mountain, Chongqing*, and relevant local floristic literature (Wang et al. 2023) were used as supplementary references during interpretation. Finally, the reconstructed species-composition map was converted into the initial-community input required by LANDIS-II (Fig. 3a).

2.3.2 Site type delineation

Topographic heterogeneity was incorporated into model initialization by combining slope, aspect, and slope position. Spatial overlay analysis was conducted in ArcMap, and areas sharing the same combination of the three variables were assigned

237 to the same site type (Zhang et al. 2025). A total of 38 site types occurred within the
238 study area (Fig. 3c, Table S1, Online Resource 1). These site types were subsequently
239 used to assign species-specific establishment and growth conditions in the LANDIS-II
240 Biomass Succession model.

241 **2.3.3 Treatment of severely disturbed and non-vegetated areas**

242 Only spatial units designated as valid succession areas were included in the
243 LANDIS-II simulations (Gao et al. 2015). Bare ground and combustion residue cells
244 were distinguished during model initialization. Bare ground cells were assigned zero
245 initial vegetation biomass. Combustion residue cells were initialized with a sparse
246 fern functional group (cohort age = 0 yr; biomass = 50 g m^{-2}) to represent incipient
247 herbaceous regeneration without assuming established woody vegetation.

248 **2.3.4 Simulation scenario design**

249 Two restoration scenarios were developed:

250 Natural succession scenario (S1) represented post-fire succession under the
251 reconstructed initial vegetation conditions without additional restoration intervention.
252 Vegetation dynamics proceeded according to the establishment, growth, biomass
253 accumulation, dispersal, competition, and replacement processes represented in the
254 LANDIS-II Biomass Succession model. Outputs from S1 were used to characterize
255 long-term natural recovery trajectories and to derive the Restoration Potential Index
256 (RPI) for long-term natural recovery potential.

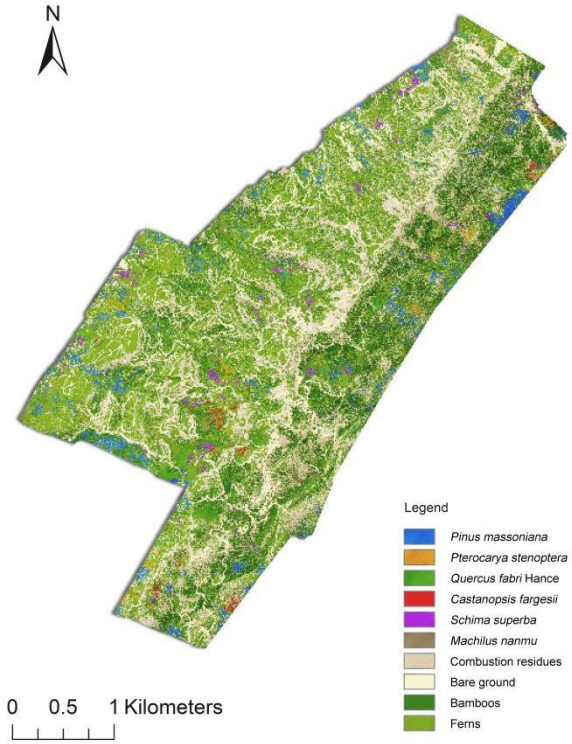
257 Targeted planting scenario (S2) represented active restoration through spatially
258 targeted planting in areas identified as having relatively low natural recovery

potential. Active planting represents a widely applied human-assisted strategy for accelerating post-fire forest recovery, particularly in severely disturbed areas where natural regeneration is limited (Rodman et al. 2024; Marsh et al. 2026). Intervention areas were defined from the RPI derived from S1 together with the corresponding post-fire vegetation and site conditions.

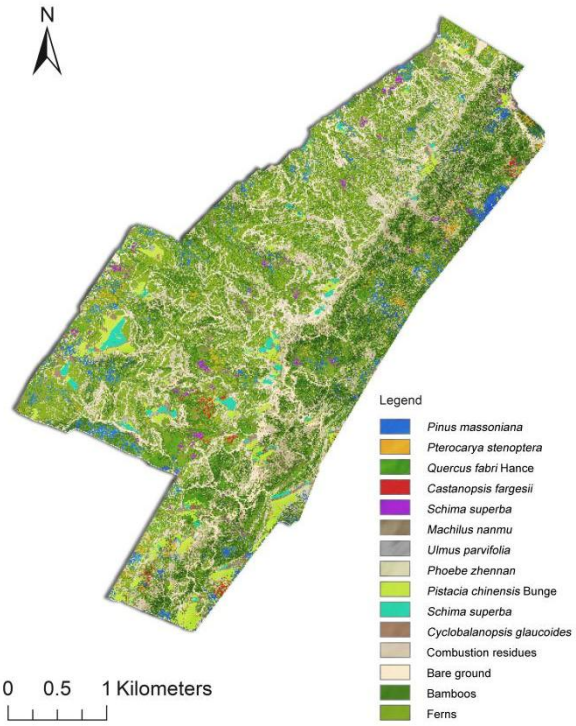
Targeted planting was implemented at simulation year 0 by assigning the RPI-defined intervention cells to restoration-specific initial-community classes. Each of the six selected tree species was introduced as a 3-year-old cohort. Initial cohort biomass was set to 800 g m^{-2} for *Pterocarya stenoptera*, *Schima superba*, *Pistacia chinensis*, and *Ulmus parvifolia*, and to 850 g m^{-2} for *Phoebe zhennan* and *Cyclobalanopsis glaucoides*. The corresponding restoration communities also retained a 3-year-old fern cohort with an initial biomass of 150 – 200 g m^{-2}, representing targeted planting within an existing post-fire regenerating vegetation matrix rather than complete replacement of the initial vegetation. Outside the intervention areas, the initial-community assignments used in S1 were retained unchanged. Planting intensity was therefore represented through cohort presence and initial cohort biomass rather than explicit stem density.

Six locally appropriate tree species were selected for planting (Table S5, A1a-f). Species selection considered (1) suitability for local site conditions; (2) documented occurrence or application in regional forest restoration; and (3) functional traits relevant to post-fire recovery, including tolerance of environmental stress, post-disturbance establishment, and contribution to longer-term forest development. S1

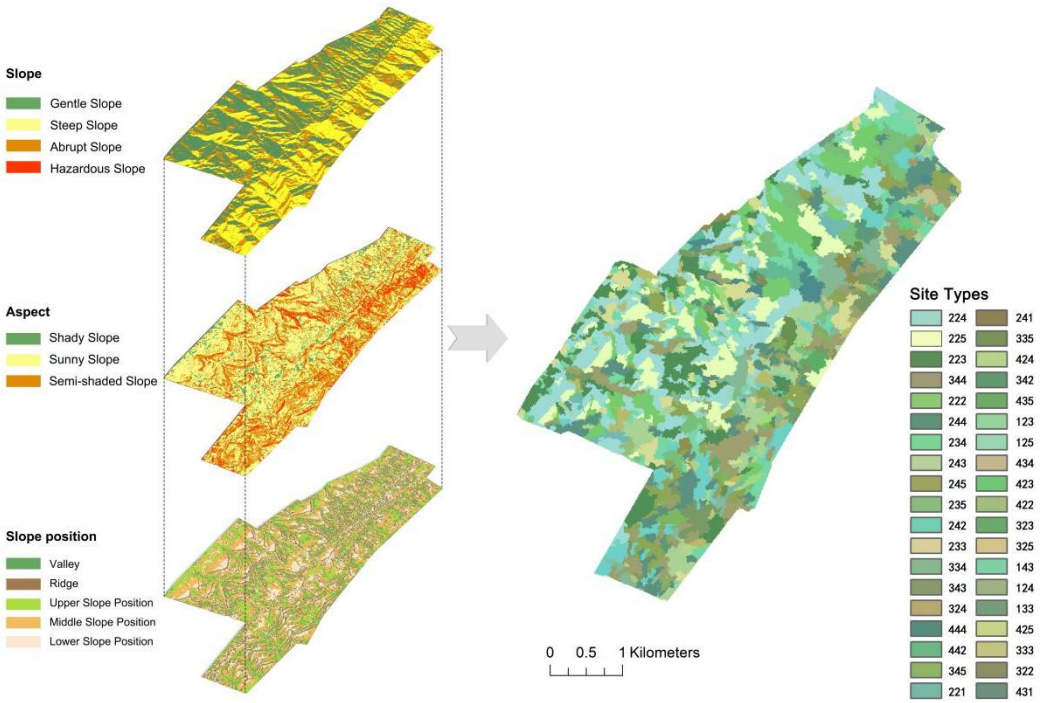
281 and S2 used the same spatial domain, site-type classification, ecoregion map, model
282 structure, and environmental parameterization; they differed primarily in the initial-
283 community assignments within the targeted intervention areas (Fig. 3b).
284



(a) Initial species and functional group composition used for S1



(b) Initial species and functional group composition used for S2



(c) Delineation of 38 site types

285 **Fig. 3** LANDIS-II spatial initialization and site-type classification. Three-digit site-

type codes represent the corresponding combination of slope class, aspect class, and slope-position class; the complete coding scheme is provided in Table S1

2.4 LANDIS-II parameterization and simulation settings

Simulations were conducted using LANDIS-II Core version 8.0 (http://www.landis-ii.org) with the Biomass Succession extension version 7.0 (https://landis-ii-foundation.github.io/Extension-Biomass-Succession/). Model inputs included the initial community data, ecoregion map, core species parameter file, and species and ecoregion specific Biomass Succession parameter files.

The core species file specified longevity, age at sexual maturity, effective and maximum seed-dispersal distances, vegetative reproduction probability, minimum and maximum sprouting ages. These parameters were compiled from published ecological literature and local floristic information (Zhou et al. 2018). The complete core parameter set for the species and functional groups represented in the simulations is provided in Table 1.

The 38 site types defined by slope, aspect, and slope position were treated as ecoregions (Pauli et al. 2015; Marcon et al. 2019). Species-specific establishment probabilities (ProbEstablish), ANPPmax, and Biomassmax were parameterized using a literature-informed and topography-adjusted approach based on published ecological information, local floristic records, field-observed species–site associations, and relative suitability across slope, aspect, and slope-position classes. Full parameterization rationale and the complete species × site-type parameter

matrix are provided in Supplementary Methods S1 and Table S2, respectively. ProbEstablish values were constrained between 0 and 1, with higher values indicating greater relative establishment suitability. Maximum ANPP (ANPPmax) and aboveground biomass (Biomassmax) were likewise varied among site types, whereas mortality probability was held constant among site types for each species. Regional background climate and soil conditions were held constant because the analysis focused on fine-scale topographic variation within the study landscape.

Table 1 Core species parameters used in the LANDIS-II simulations.

Species or functional group	Longevity (yr)	Sexual maturity (yr)	Effective dispersal distance (m)	Maximum dispersal distance (m)	Vegetative reproduction probability	Minimum sprouting age (yr)	Maximum sprouting age (yr)
Pinus massoniana	120	15	150	350	0.4	1	3
Pterocarya stenoptera	100	10	50	200	0.4	2	4
Quercus fabri Hance	350	25	20	100	0.6	3	6
Castanopsis fargesii	200	30	20	100	0.6	3	6
Schima superba	180	20	50	200	0.4	2	4
Machilus nanmu	220	25	50	300	0.4	3	6
Bamboo	60	4	5	20	0.8	1	2
Fern	20	1	3	10	0.8	0	1
Ulmus parvifolia	150	12	100	300	0.5	1	3
Phoebe zhennan	300	25	50	300	0.5	3	6

Pistacia chinensis Bunge	200	15	100	350	0.4	2	5
Cyclobalanopsis glaucoides	350	25	20	100	0.6	3	6

LANDIS-II simulations were conducted over 100 years using a 10-year succession time step. Preliminary simulations were performed at spatial resolutions of 30 and 10 m, and the 10-m resolution was retained because it better represented the fine-scale heterogeneity captured by the UAV-derived vegetation and topographic data while remaining computationally feasible.

To account for stochasticity in species establishment, dispersal, and succession, each scenario was simulated independently three times using different random-number seeds while all other model settings and parameters were held constant. Outputs from the three replicates were averaged for subsequent analyses.

2.5 Restoration Potential Index

LANDIS-II generated spatially explicit outputs of total biomass, species-specific biomass, aboveground net primary productivity (ANPP), and species composition. Pixels outside the valid simulation domain or with missing outputs were excluded, whereas zero-biomass cells within the simulation domain were retained as valid severely disturbed or early-successional states.

The Restoration Potential Index (RPI) was calculated exclusively from year-100 outputs of the natural succession scenario (S1) to characterize relative spatial

differences in modeled long-term natural recovery capacity and to support the identification of priority areas for targeted intervention (S2). The index integrated three complementary attributes of simulated ecosystem recovery (Wang et al. 2010; Zhang et al. 2018): structural recovery (SRI), represented by total biomass; functional recovery (FRI), represented by ANPP; and community structure development (CSI), represented by species richness and the relative biomass contribution of the late-successional indicator species *Castanopsis fargesii*. Detailed calculations of the three components are provided in Table 2. The baseline RPI was calculated as:

$$RPI=(0.4\times SRI)+(0.4\times \mathrm{FR}I)+(0.2\times CSI) \quad (1)$$

SRI and FRI were assigned weights of 0.40 and CSI a weight of 0.20 to place greater emphasis on structural and functional recovery while retaining community development as a complementary component. Because these weights were ecologically informed rather than empirically estimated, a sensitivity analysis was conducted using four alternative weighting schemes: equal weighting (0.333/0.333/0.333), structural emphasis (0.50/0.30/0.20), functional emphasis (0.30/0.50/0.20), and community emphasis (0.30/0.30/0.40). Each alternative RPI surface was subjected to the same spatial processing as the baseline RPI. Robustness was evaluated using pixel-wise Spearman rank correlations and by comparing the spatial overlap of the lowest-ranked 5%, 10%, and 20% of RPI cells using the Jaccard index and the proportion of baseline priority cells retained under each alternative weighting scheme (Table S3).

To reduce pixel-scale variability while preserving broader spatial patterns, the

year-100 RPI surface was spatially smoothed in ArcGIS using the median within a circular neighborhood of three cells in radius. The smoothed baseline RPI was initially classified into four classes using the Jenks natural-breaks method, with class breaks at approximately 0.34, 0.45, and 0.50. For management interpretation and graphical clarity, the two intermediate classes were subsequently merged, resulting in three recovery-potential zones: low (RPI < 0.34), moderate (0.34 ⩽ RPI < 0.5), and high (RPI ⩾ 0.5). Areas with relatively low RPI were used to identify priority intervention areas under S2.

The RPI was therefore interpreted as a model-derived, endpoint-based relative spatial prioritization metric for comparing long-term natural recovery capacity under S1, rather than as an absolute measure of restoration success.

Table 2 Definition and calculation of the Restoration Potential Index (RPI) components based on year-100 outputs of the natural-succession scenario (S1)

Component	Calculation	Definition
SRI	$SRI=\frac{B-B_{min}}{B_{ref}-B_{min}}$	Where B is the total biomass of the current pixel, B_{min} is the minimum value of the source data, and B_{ref} is the 75th percentile of the total biomass distribution.
FRI	$FRI=\frac{ANPP-ANPP_{min}}{ANPP_{ref}-ANPP_{min}}$	Where ANPP is the annual net primary productivity of the current pixel, $ANPP_{min}$ is the minimum value of the source data, $ANPP_{ref}$ is the 75th percentile of the ANPP distribution.

CSI	CSI=0.6S+0.4P	Where S is the species richness index, $S=\frac{N_{species}}{8}$, $N_{species}$ denotes the number of the eight species or functional groups represented in the S1 species pool with biomass > 0; P is the proportion of total biomass contributed by *Castanopsis fargesii*, which was used as a late-successional indicator species based on its documented role in mature evergreen broad-leaved forests and its classification as a dominant late-successional canopy species in Jinyun Mountain.

Note: For SRI and FRI, values exceeding the 75th-percentile reference were capped at 1, thereby constraining both indices to the range 0 – 1. The 75th percentile was used as an internal relative reference to reduce the influence of extreme upper-tail values rather than as an ecological threshold.

2.6 Scenario comparison and statistical analysis

Changes in total biomass and ANPP were evaluated separately for S1 and S2 using the decadal simulation outputs. A one-breakpoint piecewise linear regression was fitted to each trajectory in R using the segmented package. Breakpoints and the slopes before and after each breakpoint were estimated from the fitted curves. Because the trajectories were based on model outputs generated at 10-year intervals, the fitted breakpoint years were interpreted as descriptive estimates of shifts in simulated recovery rates rather than as exact transition times or inferential estimates.

Biomass-weighted community diversity was quantified using the Shannon-Wiener index (H’):

$$H' = -\sum_{i=1}^{S} P_i \ln(P_i) \quad (2)$$

where S is the number of species or functional groups with non-zero biomass, and P_i is the proportion of total biomass contributed by species or functional group i.

Forest carbon stock was estimated from simulated aboveground dry biomass. Carbon storage was calculated using the carbon fraction (CF) of dry biomass for each species (Table S4), obtained from authoritative forest carbon accounting references (State Forestry Administration of China 2014):

$$C = B \times CF \times 0.01 \quad (3)$$

where C represents carbon stock (t C·ha^{-1}), B represents aboveground dry biomass output from LANDIS-II(g·m^{-2}), and CF represents the carbon fraction of dry biomass. The factor 0.01 converts biomass from g m^{-2} to t biomass ha^{-1}, which was subsequently multiplied by the species-specific carbon fraction to obtain carbon stock (t C ha^{-1}).

3 Results

3.1 Baseline post-fire vegetation conditions

Approximately 21 months after the August 2022 wildfire, ferns and bamboo accounted for 45.04% and 16.09% of the study area, respectively, whereas surviving trees accounted for 6.39%. Combustion residues remained widespread (25.85%), and bare ground accounted for 6.67% of the landscape. The spatial distribution of vegetation was highly heterogeneous, with ferns and bamboo forming extensive patches and surviving trees occurring in more spatially restricted clusters (Fig. 4).

These previously characterized land-cover and vegetation patterns were used as the empirical baseline for reconstructing the initial vegetation conditions of the succession simulations.

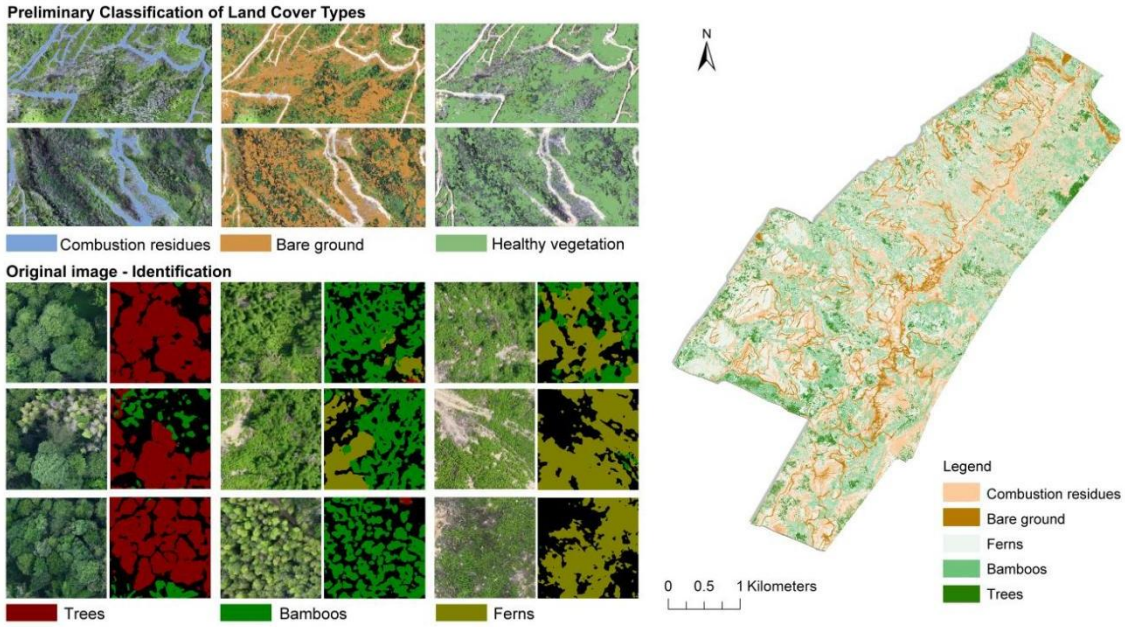


Fig. 4 Baseline post-fire land-cover and vegetation conditions used for LANDIS-II initialization, based on the UAV classification previously reported by Li et al. (2026)

3.2 Long-term biomass trajectories under natural succession

Under S1, the eight species and functional groups exhibited contrasting biomass trajectories over the 100-year simulation (Fig. 5). Fern biomass increased rapidly during early succession, reached its highest level during the middle successional period, and subsequently declined. *Pinus massoniana* and *Pterocarya stenoptera* similarly showed rapid early biomass accumulation followed by gradual declines after reaching mid-successional peaks. The broad-leaved tree species *Quercus fabri*, *Castanopsis fargesii*, *Schima superba*, and *Machilus nanmu* also generally reached

their highest biomass during the middle successional period and declined to varying degrees thereafter. Among these species, *M. nanmu* and *C. fargesii* retained comparatively higher biomass during later succession, although neither exhibited continued late-stage biomass accumulation. In contrast, bamboo was the only functional group to show sustained biomass increase throughout the simulation, reaching approximately 7,000 g m^{-2} by 2124. Thus, the S1 simulation indicated persistent bamboo expansion alongside declining or stabilizing biomass of the major tree species during later succession.

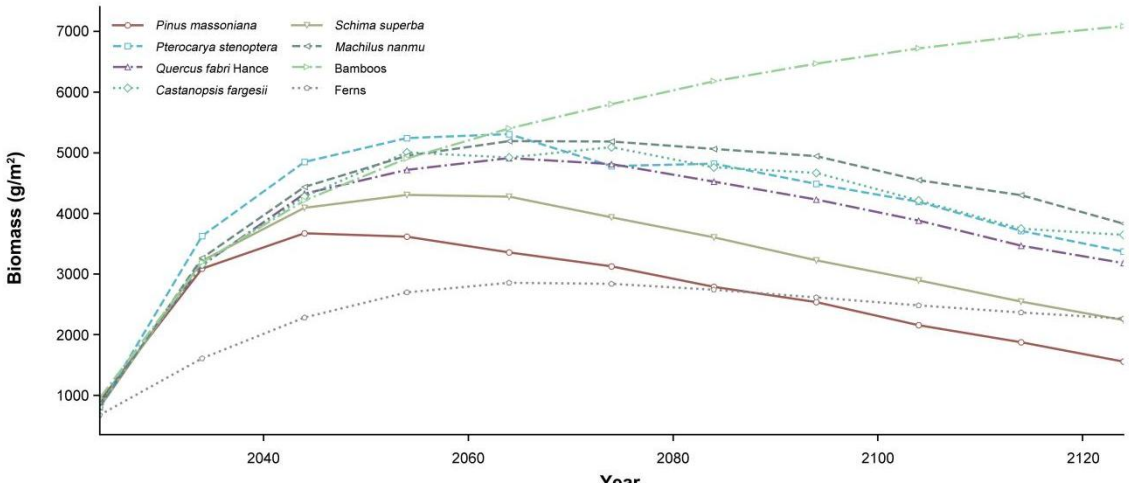
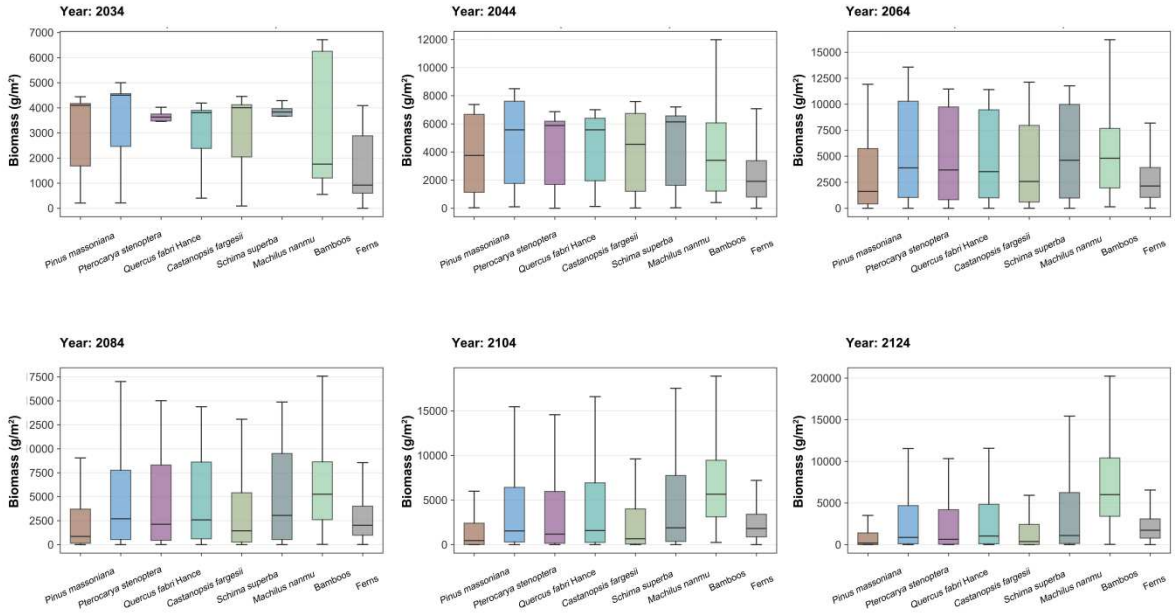


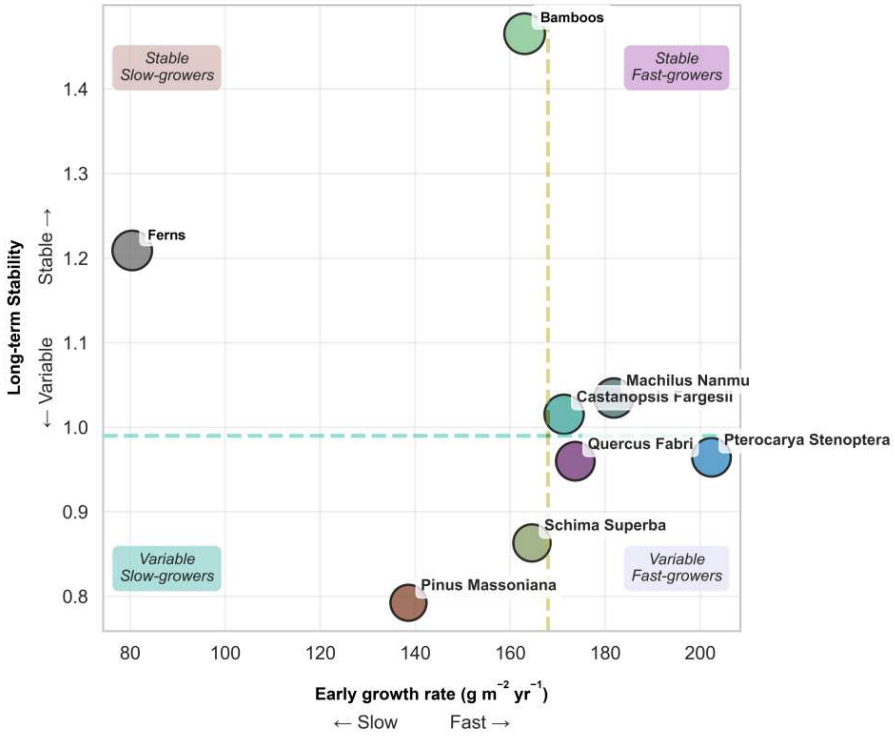
Fig. 5 100-year species biomass trajectories under natural succession

Cell-level biomass distributions further illustrated substantial heterogeneity in successional responses (Fig. 6a). During the earlier simulation stages, *P. massoniana*, *P. stenoptera*, and ferns showed relatively high biomass across many cells, whereas several broad-leaved tree species developed broader biomass distributions during the middle successional period. By the later stages, biomass distributions of most tree species shifted downward to varying degrees, while bamboo maintained high biomass

433 values across a substantial proportion of the simulated landscape. These spatial
434 distributions were consistent with the temporal trajectories shown in Fig. 5 and
435 indicated that later succession was characterized by persistent bamboo biomass rather
436 than a uniform shift toward increasing dominance of late-successional tree species.
437



(a) Distribution of simulated aboveground biomass among the eight species or functional groups at six representative stages of succession (2034, 2044, 2064, 2084, 2104, and 2124)



(b) Classification of species and functional groups according to early biomass growth rate and long-term biomass stability. Dashed lines separate the four response groups: stable slow-growers, stable fast-growers, variable slow-growers, and variable fast-growers

Fig. 6 Species biomass dynamics and successional response characteristics under S1

438

439 To further compare successional response strategies, species and functional
440 groups were characterized according to early biomass growth rate and long-term
441 biomass stability (Fig. 6b). Bamboo combined a high early growth rate with the
442 greatest long-term stability, consistent with its sustained biomass increase throughout
443 the simulation. Ferns showed a comparatively low early growth rate but relatively
444 high long-term stability, reflecting their persistence across succession despite
445 declining biomass after the middle stage. *P. massoniana* and *S. superba* showed lower
446 long-term stability, consistent with their stronger late-stage biomass declines. *P.*

447 *stenoptera* and *Q. fabri* exhibited relatively high early growth but greater temporal
448 variability. By comparison, *M. nanmu* and *C. fargesii* combined relatively rapid early
449 biomass accumulation with greater long-term stability than several other tree species.
450
451 **3.3 Spatial variation in long-term natural recovery potential**
452 The year-100 RPI revealed pronounced spatial heterogeneity in modeled natural
453 recovery capacity under S1 (Fig. 7). Following spatial smoothing and Jenks
454 classification, the original four RPI classes were consolidated into three management-
455 oriented recovery-potential zones. Low-recovery-potential areas (RPI < 0.34) were
456 concentrated in more strongly disturbed portions of the landscape and showed
457 comparatively limited recovery of vegetation structure, productivity, and community
458 development under natural succession. Moderate-recovery-potential areas (0.34 ≤
459 RPI < 0.50) generally occurred in areas characterized by mixed pioneer vegetation
460 and surviving trees, representing intermediate long-term recovery capacity. High-
461 recovery-potential areas (RPI ≥ 0.50) were more frequently associated with patches
462 containing greater surviving vegetation cover and comparatively favorable site
463 conditions, indicating stronger modeled capacity for long-term natural recovery. Low-
464 RPI areas were therefore identified as priority intervention zones for the targeted
465 planting scenario (S2).

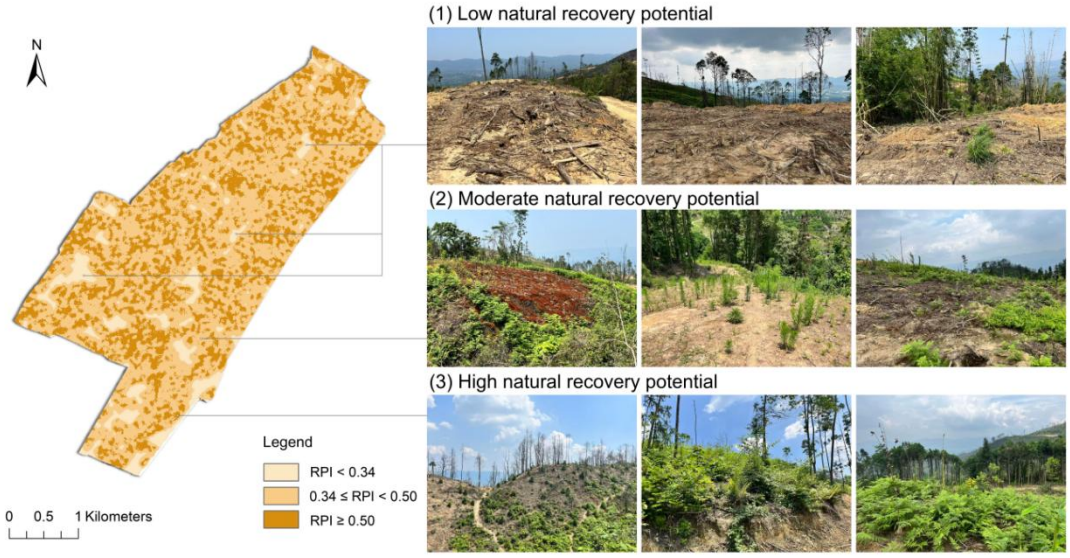


Fig. 7 Spatial variation in modeled long-term natural recovery potential under S1. The year-100 RPI surface was smoothed using a three-cell-radius circular median filter and initially classified into four classes using Jenks natural breaks. The two intermediate classes were combined to produce three management-oriented zones: low (RPI < 0.34), moderate (0.34 ≤RPI < 0.50), and high (RPI ≥ 0.50) natural recovery potential. Representative 2024 field photographs from locations falling within the three modeled recovery-potential zones are shown for spatial context

Sensitivity analysis showed that the spatial ranking of RPI was highly robust to alternative component weights, with Spearman correlations ranging from 0.967 to 0.997 relative to the baseline weighting scheme (Table S3). Across the alternative schemes, 96.3 – 97.7% of the baseline lowest-ranked 5% of cells, 96.5 – 99.5% of the lowest-ranked 10%, and 92.3 – 99.0% of the lowest-ranked 20% were retained. These results indicate that the major spatial pattern of restoration prioritization was not strongly dependent on the selected component weights.

3.4 Effects of targeted planting on long-term recovery outcomes

At simulation year 100, S2 yielded higher simulated aboveground carbon stocks than S1, with the largest positive differences concentrated primarily within the targeted planting areas (Fig. 8a). Under S1, the mean Shannon-Wiener diversity index (H') was 0.5645, indicating relatively low biomass evenness among the eight species and functional groups. Under S2, the maximum H' remained broadly comparable with that of S1, but its spatial distribution was more continuous and homogeneous (Fig. S1). Positive changes in H' occurred mainly within or near targeted planting areas, whereas slight decreases occurred in some steep-slope and ridge locations (Fig. 8b). Thus, targeted planting produced clear spatial gains in carbon stock but comparatively modest and spatially variable changes in community diversity.

The simulated biomass and ANPP trajectories also differed between scenarios (Fig. 8c, d). The fitted biomass and ANPP breakpoints occurred at approximately 45 and 46 years under S1 and at approximately 36 and 35 years under S2, respectively, corresponding to estimated advances of approximately 9 and 10 years under targeted planting. S2 also showed a steeper early recovery trajectory despite its lower initial ANPP. However, differences between the two scenarios narrowed during the middle and later stages of succession, and both trajectories became progressively less steep. These patterns indicate that the clearest effects of targeted planting occurred during earlier succession, whereas its relative advantage diminished over longer successional periods.

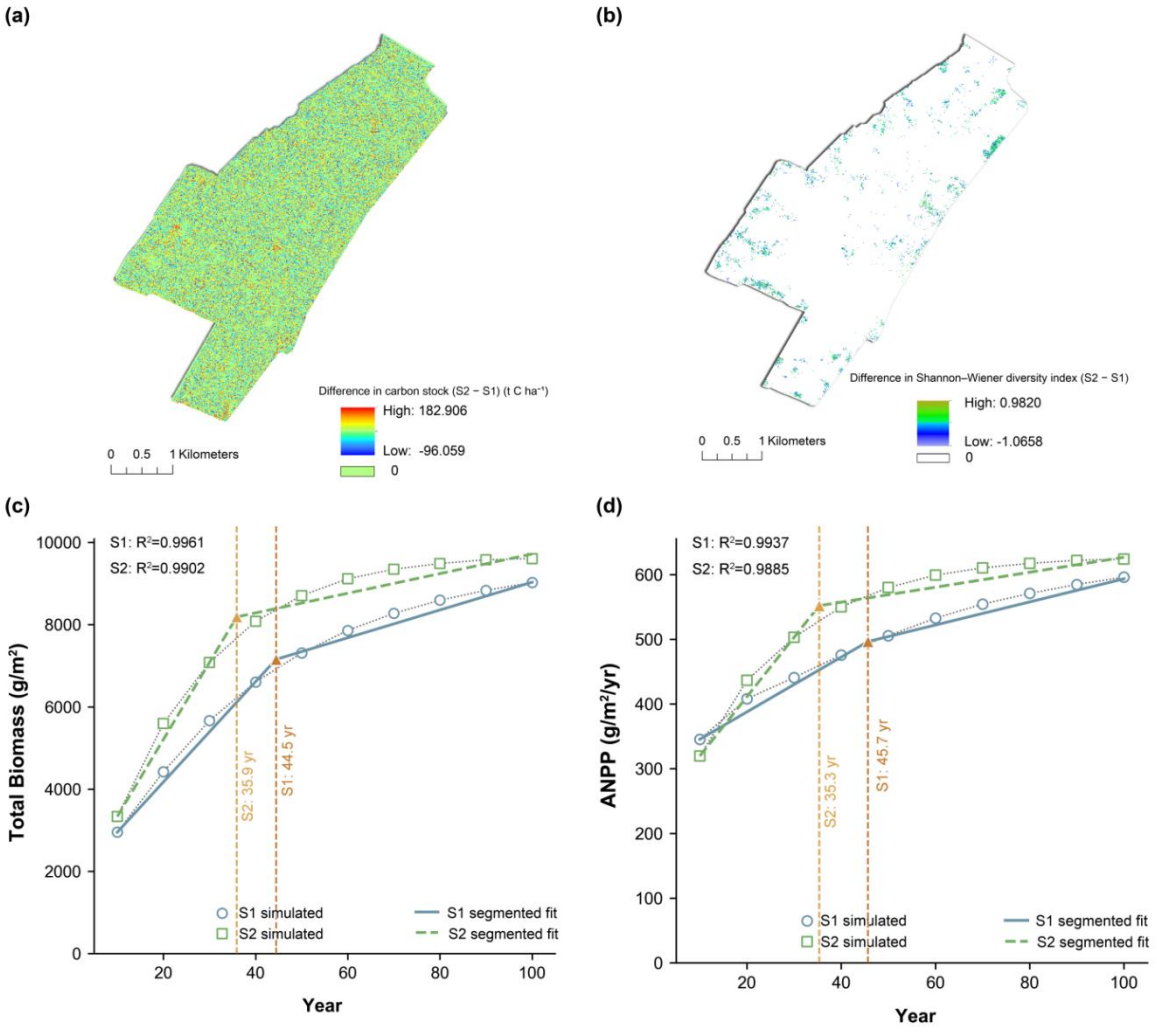


Fig. 8 Effects of targeted planting on long-term ecological outcomes and recovery trajectories. (a) Difference in aboveground carbon stock (S2−S1) at simulation year 100; (b) difference in Shannon–Wiener diversity index H′ (S2−S1) at simulation year 100; (c) simulated total aboveground biomass trajectories under S1 and S2 with segmented regression fits; and (d) simulated ANPP trajectories under S1 and S2 with segmented regression fits. Vertical dashed lines indicate estimated breakpoints

4 Discussion

4.1 Integrating fine-scale observations and succession modeling supports restoration decisions in peri-urban forests

Scientific understanding of post-fire restoration, regeneration, and succession often requires complementary observational and modeling approaches (Li et al. 2025). UAV and deep-learning methods have been widely applied to forest disturbance monitoring and vegetation feature recognition (Peris-Llopis et al. 2024; Wang et al. 2025; Wassner et al. 2025), while LANDIS-II is well established for simulating long-term landscape vegetation dynamics (Wang et al. 2010; Luo et al. 2016). Compared with single-method approaches (Sankey et al. 2017; Chen et al. 2022; Koutsias et al. 2024), the integrated framework used here provided two complementary advantages. First, high-resolution UAV imagery, U-Net classification, and field observations provided a finer empirical basis for reconstructing initial post-fire vegetation conditions for LANDIS-II. Second, the RPI translated long-term succession outputs into spatially explicit information on relative natural recovery potential, thereby linking ecological simulation with restoration prioritization.

This integration may be particularly useful in peri-urban forests, where ecological recovery takes place within heterogeneous landscapes subject to both natural disturbance and intensive management demands. Rather than applying uniform restoration across the burned area, spatial assessment of natural recovery potential allows management effort to be concentrated where intervention is most likely to be needed, while reducing unnecessary intervention in areas capable of

519 stronger natural recovery. With appropriate local calibration, the general workflow
520 may therefore be transferable to other disturbance-prone peri-urban forest systems.
521
522 **4.2 Temporal and spatial succession patterns reveal constraints on natural**
523 **recovery**
524 The simulations showed that ferns and bamboo were prominent components of
525 early post-fire recovery, consistent with secondary-succession processes in which
526 rapidly establishing vegetation can expand quickly after disturbance (Tang 2010).
527 Long-term succession under S1 further showed sustained bamboo biomass
528 accumulation throughout the simulation period. Bamboo species commonly combine
529 clonal reproduction with efficient use of above- and below-ground resources, which
530 can contribute to persistent competitive advantages in subtropical forests (Song et al.
531 2017). Similar interactions between bamboo expansion and tree regeneration have
532 been reported in disturbed tropical and subtropical forests (Ferreira et al. 2020; da
533 Silva et al. 2020; da Silva et al. 2024). In our simulations, *Machilus nanmu* and
534 *Castanopsis fargesii* retained comparatively greater long-term biomass stability than
535 several other tree species, but both declined after reaching mid-successional biomass
536 peaks. Thus, their relative stability should not be interpreted as continued late-stage
537 biomass increase. The contrasting trajectories of bamboo and tree species are
538 consistent with the possibility that persistent bamboo expansion may constrain longer-
539 term tree recovery (da Silva et al. 2024). Where such expansion conflicts with

restoration objectives, adaptive measures such as selective thinning or rhizome control may warrant consideration.

Spatial pattern is increasingly recognized as an important component of landscape-scale forest restoration planning (Rudge et al. 2022; Peris-Llopis et al. 2024; Reyes-Cedeno et al. 2025). The year-100 RPI revealed pronounced spatial heterogeneity in modeled natural recovery potential, reflecting differences in long-term structural recovery, productivity, and community development across the landscape. This is consistent with previous studies showing that post-fire recovery varies substantially along environmental and disturbance gradients (Blanco-Rodriguez et al. 2023). Building on this heterogeneity, the RPI integrated structural (SRI), functional (FRI), and community (CSI) components into a single spatially explicit prioritization metric. Low-RPI areas showed comparatively limited modeled natural recovery and were therefore prioritized for targeted intervention (Mantero et al. 2024; Rodman et al. 2024), whereas moderate- and high-RPI areas retained greater potential for assisted or passive recovery (White and Long 2019; Alayan et al. 2022; Lin et al. 2024). Accordingly, spatially differentiated restoration may be particularly relevant in peri-urban forests, where heterogeneous ecological conditions coexist with limited management resources and a continuing need to maintain forest functions within the wider urban landscape.

4.3 Targeted planting accelerates early recovery but provides diminishing long-term gains

A comparison of S1 and S2 showed that targeted planting accelerated ecosystem recovery during the early stages of succession by introducing additional tree cohorts into areas with relatively low natural recovery potential. S2 exhibited higher simulated aboveground carbon stocks and earlier biomass and ANPP breakpoints than S1, supporting previous evidence that active planting can promote early post-fire vegetation establishment and biomass recovery where natural regeneration is limited (Powers et al. 2013; Marsh et al. 2026). However, the benefits of assisted restoration were less pronounced over longer successional periods. As succession proceeded, differences in biomass and ANPP trajectories between S1 and S2 gradually narrowed, consistent with evidence that the effects of artificial and natural restoration may converge over time as endogenous ecological processes increasingly influence vegetation development (Xu et al. 2021). From a resilience perspective, this pattern suggests that active intervention may be most influential during the earlier stages of recovery, whereas natural successional processes become increasingly important as vegetation structure develops (Rodman et al. 2024).

The temporal responses of biomass and ANPP further suggest differences in the development of structural and functional attributes during succession. Under S1, the estimated ANPP breakpoint occurred slightly later than the biomass breakpoint, whereas under S2 the two breakpoints occurred at broadly similar stages. Nevertheless, the earlier biomass and ANPP breakpoints under S2 indicate that

582 targeted planting altered the timing of both structural development and ecosystem
583 productivity during early succession. This is broadly consistent with previous studies
584 showing that different dimensions of ecosystem recovery may respond at different
585 rates following disturbance (Wang et al. 2010; Escobedo et al. 2024).

586 In practice, restoration decisions should integrate multiple environmental and
587 socioeconomic factors (White and Long 2019; Rodman et al. 2024; Yue et al. 2025).
588 The effectiveness of targeted planting is highly context dependent and strongly
589 influenced by local site conditions, regeneration capacity, species selection, and
590 management objectives (Mantero et al. 2024; Zhang et al. 2025). The comparatively
591 modest and spatially variable diversity responses observed under S2 further indicate
592 that gains in biomass or carbon storage do not necessarily translate into equivalent
593 improvements in community composition. Targeted planting should therefore be
594 applied selectively rather than uniformly across the burned landscape, with greater
595 priority given to areas where modeled natural recovery potential is relatively low. For
596 post-fire management of peri-urban mountain forests, planting may also need to be
597 combined with fire prevention, continued monitoring, and adaptive management that
598 responds to changing successional conditions, including selective management of fire-
599 damaged trees, thinning, or control of dense mid-story vegetation where appropriate
600 (Busbridge et al. 2021; Yue et al. 2025).
601

4.4 Study Limitations

Several limitations should be considered when interpreting our results. First, reconstruction of initial vegetation conditions and LANDIS-II parameterization relied partly on UAV resolution, field coverage, published information, and topography-informed assumptions rather than long-term empirical calibration. Second, the RPI is a model-derived, relative endpoint-based prioritization metric rather than an absolute measure of restoration success. Although sensitivity analyses showed that the major spatial ranking and priority-area patterns were robust to alternative component weights, the index remains dependent on the selected ecological indicators, normalization procedures, and model assumptions. Third, climate change was not simulated, so century-scale trajectories should be interpreted as comparative baseline scenarios rather than deterministic forecasts. Bamboo was represented as a simplified functional group, and the magnitude of its simulated long-term expansion should therefore be interpreted cautiously. Finally, broader transferability requires evaluation across additional forest types, disturbance regimes, and peri-urban contexts, including restoration costs and socioeconomic constraints.

5 Conclusion

Post-fire recovery potential varied substantially across the Jinyun Mountain peri-urban forest. Long-term simulations showed that targeted planting in areas with relatively low natural recovery potential increased simulated aboveground carbon stocks and shifted biomass and ANPP trajectories toward earlier recovery, but its

relative advantage diminished as succession proceeded, while diversity responses remained modest and spatially variable. These findings support a spatially differentiated strategy in which active planting is concentrated where modeled natural recovery capacity is low, whereas greater reliance on passive succession is retained in areas with stronger recovery potential. Persistent bamboo expansion further highlights the need for continued monitoring and adaptive management. More broadly, integrating fine-scale post-fire observations with long-term succession modeling can provide a practical basis for allocating limited restoration resources in disturbance-prone peri-urban forests while maintaining ecological functions within the wider urban landscape.

References

Alayan R, Rotich B, Lakner Z (2022) A comprehensive framework for forest restoration after forest fires in theory and practice: A systematic review. Forests 13(9). https://doi.org/10.3390/f13091354

Alberti M, Grimm NB, Palkovacs EP, Urban MC, Verrelli BC, Anderson P, Carlen EJ, Cocciardi JM, Cook EM, Fortin M-J, Gotanda KM, Hobbie SE, Johnson MTJ, Li D, Malesis-Dahm AN, Miles LS, Munshi-South J, Roman-Palacios C, Phifer-Rixey M, Salazar-Valenzuela D, Savage AM, Snyder R, Winchell KM, Zhou Y (2026) Evolving nature-based solutions for urban resilience. Science 392(6799):701–708. https://doi.org/10.1126/science.aea9563

Avetisyan D, Velizarova E, Filchev L (2022) Post-fire forest vegetation state

monitoring through satellite remote sensing and in situ data. Remote Sens 14(24). https://doi.org/10.3390/rs14246266

Blanco-Rodriguez MA, Ameztegui A, Gelabert P, Rodrigues M, Coll L (2023) Short-term recovery of post-fire vegetation is primarily limited by drought in mediterranean forest ecosystems. Fire Ecol 19(1). https://doi.org/10.1186/s42408-023-00228-w

Bonan GB (2008) Forests and climate change: Forcings, feedbacks, and the climate benefits of forests. Science 320(5882):1444–1449. https://doi.org/10.1126/science.1155121

Busbridge S, Clarkson BD, Wallace KJ (2021) A tenuous link: Information transfer between urban ecological research and restoration practice. Urban For Urban Green 60. https://doi.org/10.1016/j.ufug.2021.127019

Chen X, Chen W, Xu M (2022) Remote-sensing monitoring of postfire vegetation dynamics in the greater hinggan mountain range based on long time-series data: Analysis of the effects of six topographic and climatic factors. Remote Sens 14(13). https://doi.org/10.3390/rs14132958

Cui ZY, Zhao FJ, Zhao S, Fei T, Ye JX (2024) Research on information extraction of forest fire damage based on multispectral UAV and machine learning. Journal of Natural Disasters 33(1):99–108. https://doi.org/10.13577/j.jnd.2024.0109 [in Chinese]

da Silva IB, Miranda PN, Anderson LO, de Jesus CVS, de Aragao LEOC, Campos CA, Salimon CI, Rodriguez AFR, Silveira M (2024) Fire effect on bamboo-

668 dominated forests in southwestern amazon: Impacts on tree diversity and forest
669 structure. Rev Bras Cienc Ambient 59. https://doi.org/10.5327/Z2176-94781755
670 da Silva SS, Numata I, Fearnside PM, de Alencastro Graca PML, Ferreira EJL, dos
671 Santos EA, de Lima PRF, da Silva Dias MS, de Lima RC, de Melo AWF (2020)
672 Impact of fires on an open bamboo forest in years of extreme drought in
673 southwestern amazonia. Reg Environ Change 20(4).
674 https://doi.org/10.1007/s10113-020-01707-5
675 Escobedo FJ, Yadav K, Ossola A, Klein R, Drury S (2024) Urban forest cover and
676 ecosystem service response to fire varies across california communities. Urban
677 For Urban Green 101. https://doi.org/10.1016/j.ufug.2024.128547
678 Ferreira E, Kalliola R, Ruokolainen K (2020) Bamboo, climate change and forest use:
679 A critical combination for southwestern amazonian forests? Ambio 49(8):1353–
680 1363. https://doi.org/10.1007/s13280-019-01299-3
681 Gao XL, Zhao PX, Hao HK, Yang YZ (2015) Simulation of forest landscape dynamic
682 change based on LANDIS-II in Huanglongshan, Shaanxi Province. Acta
683 Ecologica Sinica 35(2):254–262. https://doi.org/10.5846/stxb201311202774 [in
684 Chinese]
685 Gerwing TG, Hawkes VC, Gann GD, Murphy SD (2022) Restoration, reclamation,
686 and rehabilitation: On the need for, and positing a definition of, ecological
687 reclamation. Restor Ecol 30(7). https://doi.org/10.1111/rec.13461
688 Ghermandi L, Beletzky NA, de Torres Curth ML, Oddi FJ (2016) From leaves to
689 landscape: A multiscale approach to assess fire hazard in wildland-urban

690 interface areas. J Environ Manage 183:925–937.
691 https://doi.org/10.1016/j.jenvman.2016.09.051
692 Heidari H, Arabi M, Warziniack T (2021) Effects of climate change on natural-caused
693 fire activity in western US national forests. Atmosphere 12(8).
694 https://doi.org/10.3390/atmos12080981
695 Huang C, He HS, Liang Y, Hawbaker TJ, Henne PD, Xu W, Gong P, Zhu Z (2021)
696 The changes in species composition mediate direct effects of climate change on
697 future fire regimes of boreal forests in northeastern China. J Appl Ecol
698 58(6):1336–1345. https://doi.org/10.1111/1365-2664.13876
699 Koutsias N, Panourgia K, Nakas G, Petanidou T (2024) The importance of landscape
700 and fire-history as factors explaining post-fire vegetation recovery in a
701 mediterranean island using sentinel-2 satellite data. Sci Total Environ
702 957:177443. https://doi.org/10.1016/j.scitotenv.2024.177443
703 Li B, Lei J, Yang YT, Du CL (2026) Exploration on intelligent interpretation
704 technology in ecological restoration of forest burned area: a case study of Jinyun
705 Mountain, Chongqing. Landscape Architecture 33(5):81–87.
706 https://doi.org/10.3724/j.fjyl.LA20250519 [in Chinese]
707 Li KL, Liu ZH, Xu WR, Jiao KW, Yu Y, Lv QS, Guo WH, Zhou SY, Guan RH (2025)
708 Research progress on post-fire vegetation recovery. Chinese Journal of Ecology
709 44(12):4159–4170. https://doi.org/10.13292/j.1000-4890.202512.025 [in
710 Chinese]
711 Lin Y, Fang L, Zhou W, Qiao Z, Chang Y, Yu X, Li Y, Ren P, Xiao J (2024) Evaluating

712 the long-term effects of near-natural restoration on post-fire forest dynamics in a
713 wildland-urban interface landscape. Ecol Indic 160:111777.
714 https://doi.org/10.1016/j.ecolind.2024.111777
715 Luo X, He HS, Liang Y, Wu ZW, Huang C, Zhang QL (2016) Simulating the effects
716 of fire disturbance for predicting aboveground biomass of major forest types in
717 the Great Xing'an Mountains. Acta Ecologica Sinica 36(4):1104–1114.
718 https://doi.org/10.5846/stxb201405271089 [in Chinese]
719 Mantero G, Anselmetto N, Morresi D, Meloni F, Bolzon P, Lingua E, Garbarino M,
720 Marzano R (2024) Modeling post-fire regeneration patterns under different
721 restoration scenarios to improve forest recovery in degraded ecosystems. For
722 Ecol Manag 551. https://doi.org/10.1016/j.foreco.2023.121520
723 Marcon A, Mladenoff DJ, Grignolio S, Apollonio M (2019) Effects of forest
724 management and roe deer impact on a mountain forest development in the italian
725 apennines: a modelling approach using LANDIS-II. PLoS ONE
726 14(11):e0224788. https://doi.org/10.1371/journal.pone.0224788
727 Marsh C, Hurteau MD, Burney O (2026) Carbon stock models for early post-fire
728 reforestation efforts in the southwestern US. For Ecol Manag 605.
729 https://doi.org/10.1016/j.foreco.2026.123507
730 Mitri GH, Gitas IZ (2010) Mapping postfire vegetation recovery using EO-1 hyperion
731 imagery. IEEE Trans Geosci Remote Sens 48(3):1613–1618.
732 https://doi.org/10.1109/TGRS.2009.2031557
733 Montemagni R, De Assis IR, Sinacore K, De Oliveira Gonzaga Teixeira T, C. M.

734 Pina-rodrigues F, Cherif E (2026) Shaping the future of ecological restoration:
735 Integrating predictability and adaptive insights. Restor Ecol 34(1).
736 https://doi.org/10.1111/rec.70201
737 Pauli BP, Zollner PA, Haulton GS, Shao G, Shao G (2015) The simulated effects of
738 timber harvest on suitable habitat for Indiana and northern long-eared bats.
739 Ecosphere 6(4):1–24. https://doi.org/10.1890/ES14-00336.1
740 Peris-Llopis M, Vastaranta M, Saarinen N, Gonzalez-Olabarria JR, Garcia-Gonzalo J,
741 Mola-Yudego B (2024) Post-fire vegetation dynamics and location as main
742 drivers of fire recurrence in mediterranean forests. For Ecol Manag 568.
743 https://doi.org/10.1016/j.foreco.2024.122126
744 Powers EM, Marshall JD, Zhang J, Wei L (2013) Post-fire management regimes affect
745 carbon sequestration and storage in a sierra nevada mixed conifer forest. For
746 Ecol Manag 291:268–277. https://doi.org/10.1016/j.foreco.2012.07.038
747 Regos A (2026) A roadmap for nature-based solutions to extreme wildfires. iScience
748 29(1). https://doi.org/10.1016/j.isci.2025.114364
749 Reyes-Cedeno IG, Berger P, Sanchez CN, Coronado A, Mahichi F, Luna-
750 Villavicencio H (2025) Identification of potential areas for reforestation applying
751 the analytic hierarchy process (AHP), case study from the valley of
752 aguascalientes, mexico. J Maps 21(1).
753 https://doi.org/10.1080/17445647.2025.2529551
754 Rodman KC, Fornwalt PJ, Holden ZA, Crouse JE, Davis KT, Marshall LAE,
755 Stoddard MT, Andrus RA, Chambers ME, Chapman TB, Hart SJ, Schloegel CA,

Stevens-Rumann CS (2024) Green is the new black: Outcomes of post-fire tree planting across the US interior west. For Ecol Manag 574. https://doi.org/10.1016/j.foreco.2024.122358

Rudge MLM, Levick SR, Bartolo RE, Erskine PD (2022) Developing landscape-scale forest restoration targets that embrace spatial pattern. Landsc Ecol 37(7):1747–1760. https://doi.org/10.1007/s10980-022-01461-5

Sankey T, Donager J, McVay J, Sankey JB (2017) UAV lidar and hyperspectral fusion for forest monitoring in the southwestern USA. Remote Sens Environ 195:31–43. https://doi.org/10.1016/j.rse.2017.04.007

Sankey TTs, Tango L, Tatum J, Sankey JB (2024) Forest fire, thinning, and flood in wildland-urban interface: UAV and lidar-based estimate of natural disaster impacts. Landsc Ecol 39(3):58. https://doi.org/10.1007/s10980-024-01811-5

Scheller RM, Domingo JB, Sturtevant BR, Williams JS, Rudy A, Gustafson EJ, Mladenoff DJ (2007) Design, development, and application of LANDIS-II, a spatial landscape simulation model with flexible temporal and spatial resolution. Ecol Model 201(3–4):409–419. https://doi.org/10.1016/j.ecolmodel.2006.10.009

Sithole K, Odindi JO, Mutanga O (2018) Assessing the utility of topographic variables in predicting structural complexity of tree stands in a reforested urban landscape. Urban For Urban Green 31:121–129. https://doi.org/10.1016/j.ufug.2018.02.012

Song Q, Lu H, Liu J, Yang J, Yang G, Yang Q (2017) Accessing the impacts of bamboo expansion on NPP and N cycling in evergreen broadleaved forest in

778 subtropical China. Sci Rep 7. https://doi.org/10.1038/srep40383
779 State Forestry Administration of China (2014) Guidelines on carbon accounting and
780 monitoring for afforestation project. Afforestation and Greening Management
781 Department, State Forestry Administration of China [in Chinese]
782 Tang CQ (2010) Subtropical montane evergreen broad-leaved forests of yunnan,
783 China: Diversity, succession dynamics, human influence. Front Earth Sci
784 4(1):22–32. https://doi.org/10.1007/s11707-009-0057-x
785 Thompson MP, Rodríguez Y Silva F, Calkin DE, Hand MS (2017) A review of
786 challenges to determining and demonstrating efficiency of large fire
787 management. Int J Wildland Fire 26(7):562–573.
788 https://doi.org/10.1071/WF16137
789 van Lierop P, Lindquist E, Sathyapala S, Franceschini G (2015) Global forest area
790 disturbance from fire, insect pests, diseases and severe weather events. For Ecol
791 Manag 352:78–88. https://doi.org/10.1016/j.foreco.2015.06.010
792 Viana-Soto A, Aguado I, Salas J, Garcia M (2020) Identifying post-fire recovery
793 trajectories and driving factors using landsat time series in fire-prone
794 mediterranean pine forests. Remote Sens 12(9).
795 https://doi.org/10.3390/rs12091499
796 Wang S, Zheng X, Du Y, Zhang G, Wang Q, Han D, Zhang J (2025) Estimation of
797 short-term vegetation recovery in post-fire siberian dwarf pine (pinus pumila)
798 shrublands based on sentinel-2 data. Fire 8(2).
799 https://doi.org/10.3390/fire8020047

Wang TQ, Deng HP, Liu YF, Zheng YF, Cui XR, Wang YQ (2023) Plant species diversity and geographical distribution in Jinyun Mountain National Nature Reserve. Science of Soil and Water Conservation 21(3):94–102. https://doi.org/10.16843/j.sswc.2023.03.012 [in Chinese]

Wang Z, Daun C, Yuan L, Rao J, Zhou Z, Li J, Yang C, Xu W (2010) Assessment of the restoration of a degraded semi-humid evergreen broadleaf forest ecosystem by combined single-indicator and comprehensive model method. Ecol Eng 36(6):757–767. https://doi.org/10.1016/j.ecoleng.2010.01.006

Wassner N, Figueiredo A, Nunes AN (2025) Applying remote sensing to assess post-fire vegetation recovery: A case study of serra do açor (portugal). Fire 8(5). https://doi.org/10.3390/fire8050163

White AM, Long JW (2019) Understanding ecological contexts for active reforestation following wildfires. New For 50(1):41–56. https://doi.org/10.1007/s11056-018-9675-z

Xiao J, Liang Y, He HS, Thompson JR, Wang WJ, Fraser JS, Wu Z (2017) The formulations of site-scale processes affect landscape-scale forest change predictions: A comparison between LANDIS PRO and LANDIS-II forest landscape models. Landsc Ecol 32(7):1347–1363. https://doi.org/10.1007/s10980-016-0442-2

Xu ZY, Zhou Y, Wang SX, Wang LT, Wang ZQ (2021) U-Net for urban green space classification in Gaofen-2 remote sensing images. Journal of Image and Graphics 26(3):700–713. https://doi.org/10.11834/jig.200052 [in Chinese]

822 Yue YJ, Jia WJ, Zhang ZT, Zhao PW, Zhou M, Shu Y (2025) Research progress on
823 vegetation restoration and regeneration after forest fire disturbance and the
824 influencing factors of species diversity. Chinese Journal of Ecology 44(9):3126–
825 3134. https://doi.org/10.13292/j.1000-4890.202509.024 [in Chinese]
826 Zhang J, Cardoso FCG, Zhu H, Cheuk ML, Fischer GA, Gale SW (2025) Temporal
827 shifts in the importance of environmental factors and management interventions
828 among species in the early stages of forest restoration. J For Res 36(1).
829 https://doi.org/10.1007/s11676-025-01857-4
830 Zhang Q, Zhang T, Liu X (2018) Index system to evaluate the quarries ecological
831 restoration. Sustainability 10(3). https://doi.org/10.3390/su10030619
832 Zhou MY, You WB, Lin MJ, Liu JC, Lin XE, He DJ, Liu JS, Cai CT (2018) Dynamic
833 simulation of forest landscape succession based on LANDIS model in
834 Tianbaoyan, Fujian Province of southern China. Journal of Beijing Forestry
835 University 40(8):12–22. https://doi.org/10.13332/j.1000-1522.20180186 [in
836 Chinese]

Supplementary Files

This is a list of supplementary files associated with this preprint. Click to download.

- Table1.docx
- Table2.docx
- SupplementaryInformation.pdf